Analytical Models of Phonon–Point-Defect Scattering

Ramya Gurunathan[1,*] Riley Hanus,[1] Maxwell Dylla,[1] Ankita Katre,[2] and G. Jeffrey Snyder[1,†]

[1]*Materials Science and Engineering, Northwestern University, Evanston, Illinois 60208, USA*

[2]*Centre for Modelling and Simulation, Savitribai Phule Pune University, Pune, Maharastra, India*

Point defects exist widely in engineering materials and are known to scatter vibrational modes, resulting in reduction in thermal conductivity. The Klemens description of point-defect scattering is the most-prolific analytical model for this effect. This work reviews the essential physics of the model and compares its predictions with first-principles results for isotope and alloy scattering, demonstrating the model to be a useful metric of material design. A treatment of the scattering parameter (Γ) for a multiatomic lattice is recommended and compared with other treatments presented in the literature, which have been at times misused to yield incomplete conclusions about the system's scattering mechanisms. Additionally, we demonstrate a reduced sensitivity of the model to the full phonon dispersion and discuss its origin. Finally, a simplified treatment of scattering in alloy systems with vacancies and interstitial defects is demonstrated to suitably describe the potent scattering strength of these off-stoichiometric defects.

I. INTRODUCTION

Modeling the lattice thermal conductivity, or the heat transported through atomic vibrations, has long been important to a wide range of science and engineering applications, including thermoelectrics, thermal barrier coatings, and thermal management in electronic materials. All of these functional materials rely on doping and alloying to tune their properties, and so it is important to understand the impact of impurities and other point defects on the lattice thermal conductivity [1,2].

Peierls [3] presented one of the earliest solutions for lattice thermal conductivity in 1929 by evaluating the phonon Boltzmann transport equation, which was simplified by Callaway [4] on the basis of the relaxation-time approximation. Later, Klemens [5,6] established a theory for vibrational-mode scattering due to static imperfections in a lattice, and provided closed-form expressions for thermal conductivity versus defect concentration still used today [7]. These analytical expressions based on low-order perturbation theory are useful for routine interpretation of experimental results to determine the dominant phonon-scattering sources in a material. By calculating the relative contribution of independent scattering mechanisms such as mass disorder and local strain effects, one can determine the dominant mechanisms of scattering in a defective system to guide the design of thermal materials [8–11].

First-principles techniques were developed recently to compute the impact of point defects on thermal transport. These simulations have shown very good quantitative agreement with experiments for a range of materials and have provided useful insights regarding the mechanisms of phonon-defect scattering [12,13]. However, multiple calculations are required to compute defect structures, evaluate scattering strengths, and solve the Boltzmann transport equation for the thermal conductivity [14–17]. Often, these techniques are too expensive and system dependent for the routine modeling used to determine the dominant scattering mechanisms in a system [18]. While the first-principles methods are essential for understanding vibrational-mode properties, and in many cases elucidate limitations of analytical phonon theories, the Klemens point-defect model has proven to be highly descriptive across material systems and therefore continues to be widely used [16,18–20].

The Klemens equations are defined within the ostensibly limiting approximation of a single-atom unit cell and the Debye model, or linear phonon dispersion. However, by comparison with both first-principles results and experimental results, the predictive quality of this model is demonstrated even for complex unit-cell materials.

This paper provides a functional guide for understanding the influence of point defects on phonon transport and applying the Klemens equations to model thermal-conductivity data. In addition, it resolves discrepancies between popular representations of the mass-difference model, which have led to consistent errors in model inputs that may yield large factor differences in the predicted lattice thermal conductivity (κ_L). This study also re-evaluates

*ramyaguru@u.northwestern.edu
†jeff.snyder@northwestern.edu

the limitation of these equations with regard to the Debye-model dispersion. A mechanism is demonstrated for how the model's sensitivity to dispersion relation is, in practice, lifted, justifying the use of the model in systems with arbitrary dispersion relations.

The Klemens model predicts the ratio of the defective solid's lattice thermal conductivity to that of a reference pure solid (κ_L/κ_0). The basic functional form of the ratio is $\tan^{-1} u/u$, where the disorder scaling parameter u is related to the pure-lattice thermal-conductivity reference (κ_0), elastic properties of the host lattice through its speed of sound (v_s), the volume per atom (V_0), and a scattering parameter (Γ), which captures the lattice-energy perturbation at the defect site:

$$\frac{\kappa_L}{\kappa_0} = \frac{\tan^{-1} u}{u}, \quad u^2 = \frac{(6\pi^5 V_0^2)^{1/3}}{2k_B v_s} \kappa_0 \Gamma. \quad (1)$$

At each composition, the values of κ_0, v_s, and V_0 are linearly interpolated between the end-member properties. The perturbation caused by point defects in a lattice can be understood as a combination of a kinetic energy perturbation due to the mass difference on the defect site (ΔM) and a potential-energy distortion due to both the harmonic-force-constant difference (ΔK) and the structural distortion of nearest neighbors around the defect introduced by a site radius difference (ΔR) (see Fig. 1). Often, the mass difference will be the dominant perturbation effect at a point defect, since large site volume differences are often energetically unfavorable in an alloy system. For simplicity, the remaining equations in this section are defined for mass-difference scattering alone (Γ_M), but analogous expressions for the potential-energy terms are discussed in later sections.

Γ_M is the average mass variance in the system ($\langle \overline{\Delta M^2} \rangle$) normalized by the squared average atomic mass ($\langle \overline{M} \rangle^2$) [9, 21–23]. In the notation below, site averages are denoted by a bar, while stoichiometric averages are denoted by angular

FIG. 1. Lattice-perturbation mechanisms of a point defect include a mass difference (ΔM), a harmonic-force-constant difference (ΔK), and strain scattering from site radius difference (ΔR). Each contribution perturbs the lattice Hamiltonian (E) through a different term. T is the kinetic energy of the lattice, and U_2 and U_3 are the harmonic and anharmonic contributions to the lattice potential energy.

brackets ($\langle \rangle$).

$$\Gamma_M = \frac{\langle \overline{\Delta M^2} \rangle}{\langle \overline{M} \rangle^2}. \quad (2)$$

In a compound, these averaged quantities are most easily calculated by treating each component of the compound separately. For example, a generic compound can be expressed as $A1_{c_1}A2_{c_2}A3_{c_3}\ldots An_{c_n}$ (e.g., CaZn$_2$Sb$_2$), where An refers to the nth component (e.g., Ca, Zn, or Sb) and c_n refers to the stoichiometry of that component (e.g., 1, 2, or 2).

For each site n in the compound, Eq. (3) gives the average mass variance ($\overline{\Delta M^2}_n$) and average atomic mass ($\overline{\Delta M_n^2}$) specifically for that site, which can be occupied by a set of species indexed by i, including the host atom and any substitutional defects:

$$\overline{\Delta M_n^2} = \sum_i f_{i,n}(M_{i,n} - \overline{M_n})^2, \quad \overline{M_n} = \sum_i f_{i,n}M_{i,n}. \quad (3)$$

$\overline{\Delta M_n^2}$ is defined by a sum over i of the species site fraction ($f_{i,n}$) multiplied by the mass variance at each defect site, defined from the species mass $M_{i,n}$ and average atomic mass at that site $\overline{M_n}$ [24]. In vacancy scattering, where the perturbation emerges from both missing mass (M_{vac}) and missing bonds to nearest neighbors, a virial-theorem derivation (see Sec. V) suggests that the mass difference at the vacancy site should be $M_{i,n} - \overline{M_n} = -M_{vac} - 2\langle \overline{M} \rangle$. Finally, to derive the mass-difference scattering parameter Γ_M, the stoichiometric averages of the $\overline{\Delta M_n^2}$ and $\overline{M_n}$ values are taken [Eq. (4)] [24]:

$$\langle \overline{\Delta M^2} \rangle = \frac{\sum_n c_n \Delta M_n^2}{\sum_n c_n}, \quad \langle \overline{M} \rangle = \frac{\sum_n c_n \overline{M_n}}{\sum_n c_n}. \quad (4)$$

II. COMPARISON WITH THE POPULAR MASS-DIFFERENCE EXPRESSIONS

The mass-difference model expressed in Eqs. (3) and (4) is a reformulation of the popular equation proposed in Yang *et al.* [9], and follows the interpretation of Berman *et al.* [21]. It is recommended for conceptual clarity. This section reviews other popular interpretations of the mass-difference model to understand the conceptual differences and compare the numerical results.

A. Tamura model

The mass-difference model proposed by Tamura [23,25] preserves the dependence of the phonon relaxation times on the polarization vector and the spatial anisotropy of atomic sites within the primitive unit cell, and is frequently implemented in numerical Boltzmann-transport-equation solvers for thermal conductivity [14,16,19,20,26–29].
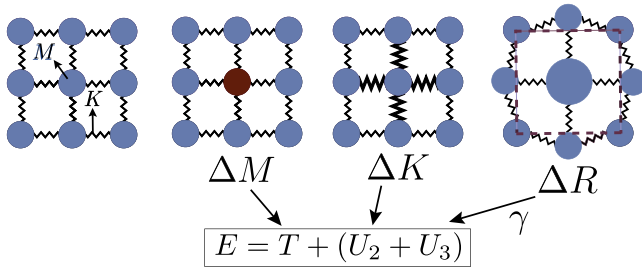
Obtaining the mass-difference parameter in the Tamura model (Γ_M^T) involves performing a sum over all the atom sites s in a simulation cell, where i again labels the species that may occupy site s, including the host and substitutional atoms. In a similar fashion to previous expressions, $M_{i,s}$ and $\overline{M_s}$ indicate the ith-species mass and the average mass on atomic site s, respectively. In this case, however, the mass-difference term is weighted by the eigenvector components corresponding to atom s in the incident $[\mathbf{e_k}(s)]$ and final $[\mathbf{e_{k'}}(s)]$ vibrational modes:

$$\Gamma_M^T = \sum_s \sum_i f_{i,s} \left(\frac{M_{i,s} - \overline{M_s}}{\overline{M_s}} \right)^2 |[\mathbf{e_k}(s) \cdot \mathbf{e_{k'}}(s)]|^2. \quad (5)$$

The eigenvectors are composed of the displacement vectors $[\mathbf{u}(\mathbf{k},s)]$ of each atomic site as it participates in a vibrational mode, weighted by the square root of the atomic mass ($\mathbf{e_k} = [\sqrt{M_1}\mathbf{u}(\mathbf{k},1) \dots \sqrt{M_s}\mathbf{u}(\mathbf{k},s)]$), and are finally normalized such that $|\mathbf{e_k}|^2 = 1$. These eigenvectors can be calculated from the density-functional-theory (DFT) force-constant matrix [30]. The description of mass-difference scattering here is general enough in its formalism that it could be used to describe the perturbation induced on a vibrational mode regardless of its spatial extent. Therefore, in addition to plane-wave phonons, the vibrational modes of diffusons, locons, and propagons within the Allen and Feldman formalism could be treated under the same point-defect-scattering theory [31,32].

Point-defect scattering has been studied with first-principles techniques by applying DFT to compute the full vibrational spectrum, using T-matrix scattering theory and the Tamura model to compute point-defect scattering rates, and finally solving the linearized Boltzmann transport equation to get κ_L [13–16,32,33]. In several reported material systems, excellent correspondence was shown between the results obtained from first-principles methods as described above and the analytical Klemens model (Fig. 2) [14,34]. It is important to remember that the Klemens model is fit to the end-member thermal conductivities but still adequately predicts the suppression of thermal conductivity with compositional variation.

In addition to the Tamura model with full structural and lattice dynamical dependence, a closed-form expression is presented for the low-frequency limit, which depends only on the atomic masses. The assumption made here is that the displacement ($\mathbf{u}$) of each atom in a low-frequency mode is roughly equal in magnitude; therefore, one can assume the magnitude of an eigenvector element is simply proportional to the square root of the atomic mass ($|\mathbf{e}(\mathbf{k},s)| \propto \sqrt{M_s}$). Following this assumption, Eq. (4) can be derived, which is detailed in Appendix A.

B. Primitive-unit-cell model

Finally, several texts, including the original descriptions by Klemens, suggest defining all parameters of the mass-difference model on the basis of the primitive unit cell [5,7,21,37,38]. Physically, this treatment suggests a monatomic lattice approximation in which the atoms of the unit cell are simply summed together in a single large, vibrating mass. The scattering strength of the lattice can be thought of as an ensemble average of its microstates, or the primitive unit cells which compose it. Therefore, the unit-cell-model mass scattering parameter (Γ_M^{UC}) can be calculated from the fraction (P_c) of unit cells with a mass of M_c and their deviation from the average unit-cell
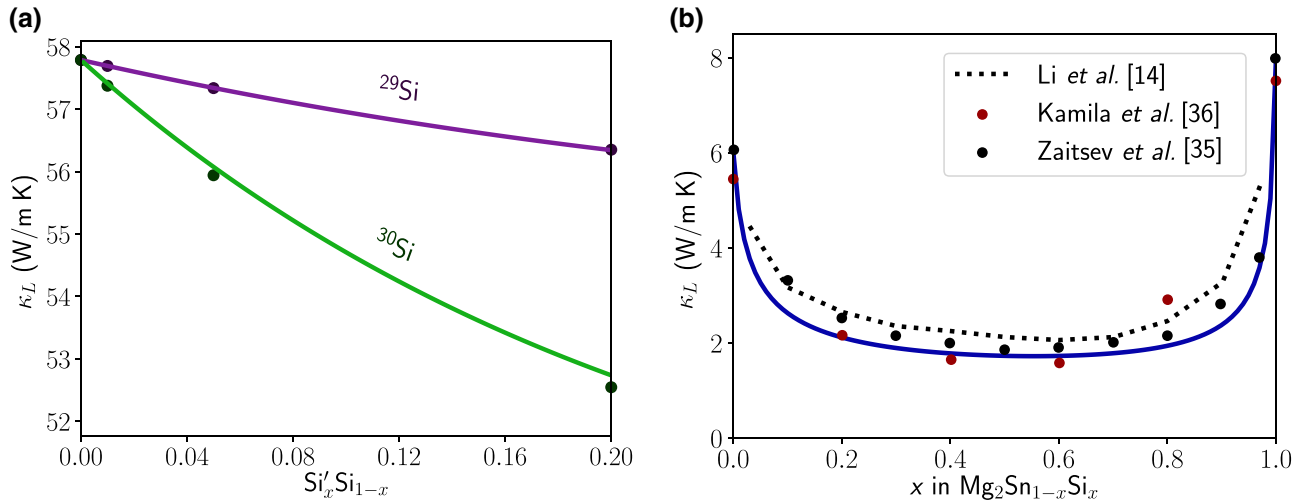

FIG. 2. Thermal-conductivity reductions due to point-defect scattering for two systems: (a) Si-isotope scattering at 800 K based on DFT dispersions and T-matrix scattering theory (points) and the Klemens model (lines) and (b) Mg$_2$Sn$_{1-x}$Si$_x$ scattering from experiments (points), T-matrix theory (dotted line), and the Klemens model (solid line) at 300 K [14,35,36].
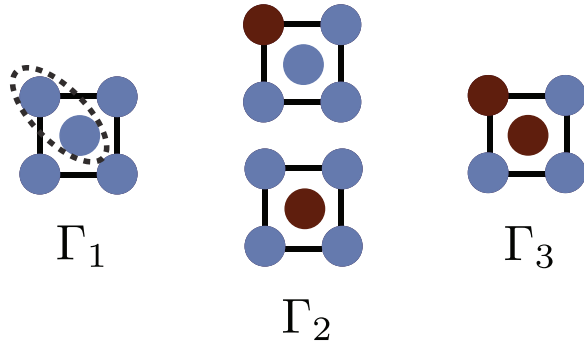
FIG. 3. In an example two-atom primitive unit cell (shown in a dotted line), three possible microstates exist, containing zero, one, or two impurity atoms. In the unit-cell basis, each microstate will contribute a term to the overall scattering parameter (Γ).

mass ($\overline{M}$). Finally, the mass differences are summed over all possible microstates in the lattice:

$$\Gamma_M^{UC} = \sum_c P_c \left(\frac{M_c - \overline{M}}{\overline{M}} \right)^2. \tag{6}$$

While most model inputs are well defined, it is not immediately clear what the fraction of unit cells (P_c) should be. When there is a random distribution of defects in the lattice, the fraction or probability of finding a unit cell of mass M_c can be determined from a binomial-distribution function (described in more detail in Appendix D). A schematic of possible unit cells (microstates) for a two-atom unit cell is shown in Fig. 3. In the case where all microstates are equally likely, the results are exactly equivalent to those produced by Eq. (4), which is more easily implemented. The benefit of the primitive-unit-cell interpretation arises when defect complexes are present in the lattice. Recent studies have identified these defect complexes in important engineering materials, including clustering of Na dopant atoms in PbTe, antisite defects occurring in close proximity in BAs, vacancy clusters in crystalline Si, and Schottky and Frenkel defect pairs in functional oxides [39–41]. In these scenarios, the microstates corresponding to the defect complexes can be preferentially weighted with a larger fraction (P_c).

C. Inconsistent usage

The dual formalisms of the scattering parameter Γ based on either "per-unit-cell" or "per-atom" quantities have led to inconsistencies in the calculation of κ_L in Eq. (1). Notably, the relevant scatterer volume for the primitive-unit-cell formalism is the volume of the primitive unit cell (V_{UC}) not the volume per atom (V_0), because this model treats one large mass per unit cell [5,23]. This value enters the phonon scattering rate [Eq. (12)] and, therefore, the κ_L prediction. The primitive-unit-cell formalism

for Γ, while suggested in several seminal papers, is rarely implemented to calculate thermal conductivity [5,7,23,37, 42,43]. Instead, Γ is most-often computed from Eq. (4) based on "per-atom" quantities. In some of these studies, however, the primitive-unit-cell volume, instead of the volume per atom, is used to calculate the disorder parameter u in Eq. (1), which leads to an overprediction of the lattice thermal-conductivity reduction (see Appendix E) proportional to the number of atoms in the unit cell [8,44–46]. Often, as discussed in Sec. V on vacancies and interstitial defects, there is a cancellation of errors such that the general conclusions of these papers about the influence of point-defect scattering in their system is still supported [8,44–47]. This effect is discussed in greater detail in Sec. V on the large scattering strength of vacancies and interstitial defects.

III. MODEL DERIVATION: UMKLAPP-SCATTERING AND POINT-DEFECT-SCATTERING TREATMENTS

This section reviews the full derivation of the Callaway-Klemens model to generalize beyond mass-difference scattering alone, clarify assumptions made in the derivation, and discuss the model's dependence on phonon dispersion, a topic attracting interest recently [18,48].

Lattice waves, or phonons, carry a substantial amount of heat through the lattice, characterized by the lattice thermal conductivity (κ_L). The efficiency of a phonon with frequency ω at transporting heat is characterized by its heat capacity (C_s), group velocity ($v_g = d\omega/dk$), and relaxation time (τ). The lattice thermal conductivity can then be expressed in terms of these values by integration over the phonon frequency up to the maximum frequency supported by the lattice (ω_m) [4,49]. If the high-temperature approximation is made, the heat capacity at frequency ω directly relates to the density of states [$g(\omega)$] as $C_s(\omega) = k_B g(\omega)$, and

$$\kappa_L = \frac{1}{3} \int_0^{\omega_m} C_s(\omega) v_g(\omega)^2 \tau(\omega) d\omega. \tag{7}$$

The relaxation time of the phonons is limited by the scattering sources in the crystalline material. Each main source of scattering has an associated relaxation time, including boundary scattering off planar defects (τ_b), umklapp phonon-phonon scattering (τ_u), and point-defect scattering (τ_{PD}). Their associated scattering rates are summed according to Matthiessen's rules ($\tau^{-1} = \tau_b^{-1} + \tau_u^{-1} + \tau_{PD}^{-1}$), assuming that the scattering mechanisms are uncoupled. The model for alloy scattering typically used to describe trends of thermal conductivity versus alloy composition ignores boundary scattering, and yields total relaxation time $\tau = \tau_u \tau_{PD}/(\tau_u + \tau_{PD})$. Finally, the model is best applied above the Debye temperature of the material, where the influence of the normal,

momentum-conserving phonon interactions on thermal conductivity can be ignored [4,6,50].

The scattering rate from a static imperfection can be derived with use of Fermi's golden rule to define the transition probability ($W_{\mathbf{k},\mathbf{k}'}$) from an initial state ($\mathbf{k}$) to a final state ($\mathbf{k}'$). The transition probability is related to the square of the perturbation-matrix element, a measure of the overlap between two phonon states induced by a perturbation of the lattice energy, and includes a lattice-energy-conservation criteria captured by $\delta(E - E')$. This transition probability is then summed over all possible final phonon states ($\mathbf{k}'$), restricted by the conservation conditions of the phonon interaction:

$$W_{\mathbf{k},\mathbf{k}'} = \frac{2\pi}{\hbar} \langle \mathbf{k} | H' | \mathbf{k}' \rangle^2 \delta(E - E') \qquad (8)$$

The three contributions to point-defect scattering (Fig. 1) introduced above are mass change (ΔM), force-constant change (ΔK), and radius change (ΔR), and each perturbs a different term in the lattice Hamiltonian (H)—the kinetic energy (T), the harmonic potential energy ($U_{2\text{nd}}$), and the third-order, anharmonic potential energy ($U_{3\text{rd}}$), respectively [5,15,51–54]. The energy perturbation (H') induced by the point defect on site $\mathbf{r}$ with a set of linkages to nearest-neighbor sites ($\mathbf{b}_n$) is then a combination of the effects discussed above:

$$H' = \frac{1}{2}\Delta M \left(\frac{d\mathbf{u}(\mathbf{r})}{dt} \right)^2 + \sum_n \frac{1}{2}\Delta K_{\mathbf{b}_n}[\mathbf{u}(\mathbf{r}) - \mathbf{u}(\mathbf{r} - \mathbf{b}_n)]^2$$

$$+ \sum_n \gamma\, \boldsymbol{\eta}(\Delta R)[\mathbf{u}(\mathbf{r}) - \mathbf{u}(\mathbf{r} - \mathbf{b}_n)]^2. \qquad (9)$$

The scattering due to local, static strain ($\boldsymbol{\eta}$) depends on the anharmonicity of the distorted bonds, as captured in the Grüneisen parameter (γ). Notably, the ΔK and ΔR effects are both captured in the changes to the DFT-calculated interatomic force constants, which change locally in response to both structural relaxation and an altered chemical environment [15]. Additionally, the strain scattering strength is scaled by the coefficient Q, which approximates the number of distorted nearest-neighbor bonds around a point defect. Assuming a cubic lattice with a strain field that decays with distance cubed, $Q = 4.2$. If all three effects are present in a system, they combine according to Eq. (10), where, as before, atomic species are indexed with i and atomic sites in the unit cell are indexed with n [5,53]:

$$\Gamma_n = \sum_i f_i \left[\frac{\Delta M^2}{\langle \overline{M} \rangle^2} + 2 \left(\frac{\Delta K}{\langle \overline{K} \rangle} - 2Q\gamma \frac{\Delta R}{\langle \overline{R} \rangle} \right)^2 \right], \quad \Gamma = \langle \Gamma_n \rangle. \qquad (10)$$

The change in force constant (ΔK) is not an intuitive value, but it is typically assumed that force constants

change proportionally with atomic volumes. Therefore, the force-constant difference and local strain terms are combined, and both are captured by the average change in atomic radius, defined analogously to the mass scattering parameter in Eqs. (3) and (4). Again, the atomic radius change on the nth site is based on the difference between the atomic radius of the ith species that can occupy that site $R_{i,n}$ and the average atomic radius of the site $\overline{R}_n$. Since the relationships between force constants and atomic volumes are system dependent, these effects are captured in a phenomenological fitting parameter ϵ, which can take a broad range of values (i.e. between 1 and 500) in order to fit to experimental data:

$$\Gamma = \frac{\langle \overline{\Delta M^2} \rangle}{\langle \overline{M} \rangle^2} + \epsilon \frac{\langle \overline{\Delta R^2} \rangle}{\langle \overline{R} \rangle^2} \quad \langle \Delta R^2 \rangle = \left\langle \sum_i f_i (R_{i,n} - \overline{R}_n)^2 \right\rangle. \qquad (11)$$

For the point-defect scattering rate (τ_{PD}^{-1}), only two phonon states, an incident and a final state, are involved in the interaction. Given the conservation-of-energy condition, the frequencies of the final and initial phonons are equal. Therefore, the sum over all final scattering states contributes the three-dimensional density of states (g) at the phonon frequency ω [24]:

$$\tau_{\text{PD}}^{-1} = \frac{V_0 \pi \Gamma \omega^2 g(\omega)}{6}, \quad g(\omega) = \frac{3\omega^2}{2\pi^2 v_p^2(\omega) v_g(\omega)}. \qquad (12)$$

In umklapp scattering, phonons scatter other phonons by virtue of the lattice distortions they generate. The scattering strength is, then, also related to the anharmonicity of the distorted bonds via the Grüneisen parameter, γ, in addition to the phase velocity of the phonon producing the distortion [$v_p(\omega) = \omega/k$] and the group velocity of the final phonon state [$v_g(\omega'')$] [3,24]. Umklapp scattering is referred to as a three-phonon process, and in the typical picture, either two incident phonons combine to form a final phonon state or an initial phonon splits into two final phonon states. Unlike normal three-phonon processes, umklapp processes do not conserve momentum, but instead include an exchange of momentum with the crystal lattice, which, given periodicity constraints, must occur in intervals of a reciprocal-lattice vector ($b = 2\pi/a$). The relevant conservation law is then $\mathbf{k} + \mathbf{k}' = \mathbf{k}'' + \mathbf{b}$. This more-complex conservation law yields a less-intuitive set of final available phonon states, and the numerical prefactor of the umklapp scattering rate varies somewhat from source to source, depending on the level of complexity assumed for the expression of final states [2,24,55,56]:

$$\tau_u^{-1} = \frac{4\pi a \gamma^2 \omega^2 k_B}{\sqrt{2} M v_p^2(\omega) v_g(\omega'')} T. \qquad (13)$$

The umklapp scattering rate appears to have the same motif present in the density of states: $\omega^2/(v_p^2 v_g)$. However, because of the increased complexity of the energy and momentum conservation in a three-phonon process, the sum over final phonon states does not simply contribute the one-phonon density of states g. Rather, the selection rule for three-phonon processes is more accurately captured by a calculation of the joint density of states, representing allowed phonon transitions, weighted by the equilibrium occupation numbers of the phonon modes $\mathbf{k}'$ and $\mathbf{k}''$ [57]. In the Klemens model, the approximation is made that the magnitude of the final phonon wave vector (k'') is small with respect to a reciprocal-lattice vector, and, as such, the phase space for final phonon states approaches the one-phonon density of states, contributing the factor $g(\omega)$ to the umklapp scattering rate [57].

At this point it is typical to make the Debye approximation, which suggests that v_g and v_p are independent of frequency and equal to the classical speed of sound ($v_s = d\omega/dk|_{k\to 0}$). Equation (7) for lattice thermal conductivity simplifies, after substitution of the expressions for relaxation time and specific heat, to the integral form of arctan and gives the final expression for κ_L shown in Eq. (1).

IV. DISPERSION-RELATION SENSITIVITY

The formalism above has shown wide applicability to thermoelectric materials, which often have complex, non-Debye dispersions. The examples of Si-isotope scattering and $Mg_2Si_{1-x}Sn_x$ scattering shown in Fig. 2 both show good correspondence between the first-principles methods and the Klemens model. Since for both materials there is disagreement with the Debye-model dispersion implicitly assumed in the Klemens theory, the suitability is surprising [58,59].

Previous studies explicitly compared the κ_L predictions of the Klemens model using various approximations of the phonon dispersion relation, ranging from the Debye model to polynomial or trigonometric fits of the dispersion [18,48]. For example, in a study of two half-Heusler systems, three different approximations were used to describe the phonon structure of the two materials—the Debye model, a truncated Debye model, and a cubic polynomial fit of the full dispersion relation. The predicted κ_L-versus-defect-concentration curve was plotted for each case and compared with experimental results. The study showed that the prediction of the pure thermal conductivity (κ_0) depended on the choice of dispersion. However, the ratio κ_L/κ_0 was shown to be independent of the dispersion-relation choice, suggesting that while full features of the dispersion relation are required to model the thermal conductivity of pure solids, the suppression of κ_L due to point defects can be described more generally [18].

The dispersion-relation dependence enters the Klemens model through the factors of density of states and the frequency-dependent phonon velocities. In Eq. (14) for lattice thermal conductivity, the relaxation times are rewritten to isolate the contribution of the density of states [$\tau_{\mathrm{PD}}^{-1} = a\,g(\omega)\omega^4, \tau_u^{-1} = b\,g(\omega)\,\omega^2$], with coefficients a and b combining any physical and material constants:

$$
\kappa_L = k_B \int_0^{\omega_m} v_g^2(\omega)g(\omega)\omega^2 \frac{[1/b\,g(\omega)]\omega^2}{1 + a\,g(\omega)\omega^2/b\,g(\omega)}d\omega
$$
$$
= \frac{k_B}{b} \int_0^{\omega_m} v_g^2(\omega)\frac{1}{1 + a\omega^2/b}\,d\omega. \tag{14}
$$

The factor $g(\omega)$ cancels in each of the relaxation times as well as the heat capacity, softening the dispersion dependence of the expression. A full derivation of this form is given in Appendix C.

At this point, the factor v_g^2 remains as a phonon-structure-related quantity in the model. Therefore, the dispersion dependence is not eliminated from the model, but is softened.

However, the partial cancellation of dispersion-relation quantities through the factors of density of states in the model inputs helps justify this model's application to a wide range of complex, functional electronic materials.

V. SCATTERING DUE TO VACANCIES AND INTERSTITIAL DEFECTS

The Klemens-Callaway model is best defined for randomly dispersed substitutional defects. However, initial work on other off-stoichiometric defects, including vacancies and interstitial defects, showed large phonon-scattering effects and these warrant further investigation.

Several investigations of thermoelectric compounds show large thermal-conductivity reductions due to vacancy scattering [44–47,60–63]. In several of these cases, the reduction in κ_L is attributed to mass-difference scattering alone. However, it was identified that the volume in Eq. (12) was incorrectly defined as the volume of the unit cell rather than the volume per atom, leading to overprediction of the thermal-conductivity change [8,44–47].

However, the large perturbation effects of vacancies are still well described by the Klemens theory [64,65]. In this case, the lattice-energy perturbation comes from missing kinetic energy (T') related to the mass of the removed atom and missing potential energy related to the removed bond between two atoms, or double the potential energy per atom ($2U'$). Within the harmonic approximation ($E = T + U_{2\mathrm{nd}}$), the kinetic-energy and potential-energy perturbations of a single atom should be equal ($T' = U'$) according to the virial theorem, allowing one to relate the potential-energy perturbation to the average atomic mass in the lattice ($\overline{\langle M\rangle}$). In the calculation of Γ, the perturbation at a vacancy site can be represented by the mass
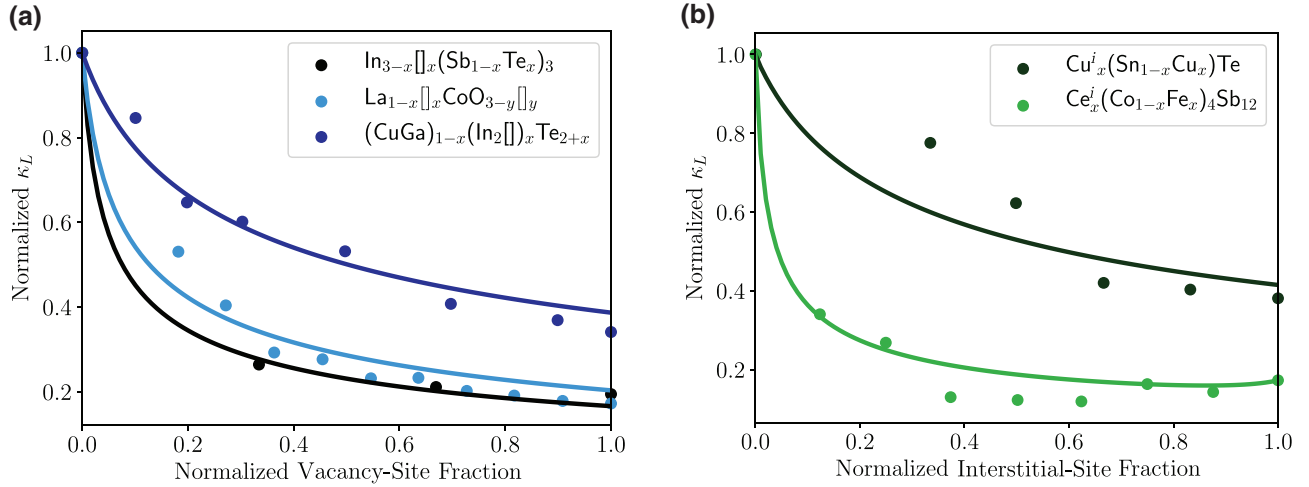
FIG. 4.   Both vacancy-site-scattering data and interstitial-site-scattering data from the literature (points) can be described by a simple treatment of broken (or added) bonds based on the virial theorem (line). Normalized thermal-conductivity reductions for systems with (a) stoichiometric vacancies, where [] represents a vacancy [44,45,62] and (b) stoichiometric interstitial atoms [8,66].

difference $M_{i,n} - \overline{M_n} = -M_{vac} - 2\langle\overline{M}\rangle$ in Eqs. (4) and (5), where M_{vac} is the mass of the vacant atom [64,65].

This simple treatment of vacancy scattering performs well in many defective solids, some of which are reproduced in Fig. 4(a). The experimental data shown would not be described by standard mass difference alone and require the perturbation induced by a missing bond. Results for the mass-difference-only curve versus the full inclusion of the term for broken bonds are compared in Appendix E, which shows how an incorrect definition of volume can lead to a cancellation of errors.

The suitability of the vacancy model suggests that interstitial atoms may be describable with an identical treatment. Interstitial or filler atoms represent the reverse situation, where an extra mass (M_{int}) is added onto a site and a new bond forms between the interstitial atom and a neighbor; therefore, a perturbation of $T' + 2U'$ should apply, yielding essentially the same mass difference as before $(M_{i,n} - \overline{M_n} = M_{int} + 2\langle\overline{M}\rangle)$. The interstitial-atom sites have a stoichiometry corresponding to the ratio of interstitial sites to lattice sites. While interstitial scattering requires more-detailed study across additional material systems, the initial data represented in Fig. 4(b) support the application of the virial-theorem treatment.

VI. CONCLUSION

The analytical point-defect-scattering model provides a simple route to identify scattering mechanisms in a system. In several systems, comparisons of alloy scattering models with different scattering terms excluded, such as strain scattering or broken bonds, provide a lens into the most-potent scattering effects and a route to optimally tailor the thermal properties via defect engineering [8,41,46,66]. The systems best described by this model

are those with well-defined crystal structures, randomly dispersed point defects, and low-magnitude perturbations, such that regions of high mass contrast and high defect concentration may require verification [19]. However, the large thermal-conductivity reduction induced by vacancies and interstitial atoms is still described by these analytical equations using the virial theorem to model the perturbation due to the formation or removal of nearest-neighbor bonds.

In addition, the suitability of the alloy model for arbitrary dispersion relations suggests that the ratio of alloy scattering to umklapp scattering predicted by the model is fairly dispersion relation independent. This reduced sensitivity to dispersion can be understood through a partial cancellation of the density of states in the phonon relaxation times and heat capacity. As a result, it is found that these equations are justifiable in describing the impact of point defects on the thermal properties of materials with complex atomic and phonon structures attracting attention in fields such as thermoelectrics and microelectronics.

APPENDIX A: TAMURA-MODEL LOW-FREQUENCY LIMIT

This section describes the low-frequency approximation of the Tamura model. The Tamura expression with full

structural and lattice dynamical dependence is given in Eq. (5) and is reproduced below:

$$\Gamma_M^T = \sum_s \sum_i f_{i,s} \left(\frac{M_{i,s} - \overline{M_s}}{\overline{M_s}} \right)^2 |[\mathbf{e_k}(s) \cdot \mathbf{e_{k'}}(s)]|^2. \quad (A1)$$

In addition, an approximation is described in the low-frequency limit to yield a closed-form expression, which depends only on the atomic masses. The assumption made here is that the displacement (**u**) of each atom in a low-frequency mode is roughly equal in magnitude; therefore, the magnitude of an eigenvector element is proportional to the square root of the atomic mass [$|\mathbf{e}(\mathbf{k}, s)| \propto \sqrt{M_s}$]. This suggests that the squared polarization vector dot product $\{|[\mathbf{e_k}(s) \cdot \mathbf{e_{k'}}(s)]|^2\}$ weights the mass difference on a site depending on its mass relative to the other atoms in the formula unit, or an approximate factor of $(\overline{M_s}^2/\langle \overline{M} \rangle^2)$. This treatment results in Eqs. (3) and (4), as depicted below:

$$\Gamma_M^{LF} = \frac{1}{\langle \overline{M} \rangle^2} \frac{\sum_n c_n (\overline{M_n})^2 \sum_i f_i (1 - M_{i,n}/\overline{M_n})^2}{\sum_n c_n} = \frac{\langle \overline{\Delta M^2} \rangle}{\langle \overline{M} \rangle^2}. \quad (A2)$$

In the original paper by Tamura, the low-frequency limit is instead

$$\Gamma_M^{LF} = \frac{\sum_n c_n (\overline{M_n})^2 \sum_i f_i (1 - M_{i,n}/\overline{M_n})^2}{\sum_n c_n \overline{M_n}^2}$$

$$= \frac{1}{\langle \overline{M}^2 \rangle} \frac{\sum_n c_n \Delta M_n^2}{\sum_n c_n} \quad \langle \overline{M}^2 \rangle = \frac{\sum_n c_n \overline{M_n}^2}{\sum_n c_n}. \quad (A3)$$
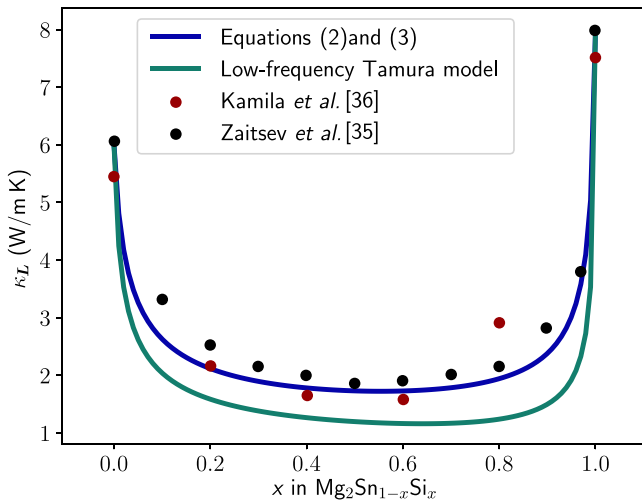

FIG. 5. The predictions of the low-frequency Tamura model and Eqs. (3) and (4) are compared for the example of point-defect scattering in a $Mg_2Sn_{1-x}Si_x$ solid solution. The low-frequency Tamura model typically overpredicts the thermal-conductivity reduction due to point-defect scattering.

As shown, this expression can be rearranged to a form similar to Eq. (4). However, the expression is subtly different, as it includes an averaging of the squared atomic masses ($\langle \overline{M_n}^2 \rangle$), rather than the average mass, which is finally squared ($\langle \overline{M_n} \rangle^2$). Through comparison with experimental and simulated thermal-conductivity data, the mass-difference term provided in Eq. (4) is verified to give more accurate predictions, while Eq. (A3) can deviate by 30%–40%. Figure 5 compares the results obtained with the low-frequency Tamura model and Eq. (4) for a $Mg_2Sn_{1-x}Si_x$ solid solution. Moreover, the mass-difference parameter from Eq. (A3) suffers from a lack of generalizability to arbitrary unit cell sizes, such that a doubling of the unit cell leads to an increase in the predicted scattering rate.

APPENDIX B: DERIVATION OF RELAXATION TIMES

This section details the derivations of the point-defect and umklapp relaxation times from Fermi's golden rule to understand their dependence on phonon velocity and the dispersion relation.

1. Point-defect scattering

Point defects act as a static perturbation, and therefore the scattering rate can be determined using Fermi's golden rule based on first-order perturbation theory. Previous work showed that higher-order perturbation terms have negligible effects on the lattice energy [25,26]. The probability of scattering from state **k** to state **k'** ($W_{\mathbf{k},\mathbf{k'}}$) is proportional to the square of the perturbation-matrix element, a measure of the overlap between two phonon states due to a perturbation of the lattice energy, with conservation of energy enforced through the $\delta(\omega_\mathbf{k} - \omega_{\mathbf{k'}})$ term:

$$W_{\mathbf{k},\mathbf{k'}} = \frac{2\pi}{\hbar^2} \langle \mathbf{k} | H' | \mathbf{k'} \rangle^2 \delta(\omega_\mathbf{k} - \omega_{\mathbf{k'}}). \quad (B1)$$

The perturbation-matrix element includes a coefficient (C) that captures the physics of the perturbation induced by the point defect, while $a(\mathbf{k})$ and $a^*(\mathbf{k'})$ are creation and annihilation operators to represent the change in occupation numbers of the **k** and **k'** states as a result of the phonon-impurity interaction:

$$\langle \mathbf{k} | H' | \mathbf{k'} \rangle = C(\mathbf{k}, \mathbf{k'}) a(\mathbf{k}) a^*(\mathbf{k'}) \quad (B2)$$

Substitution of the full form of the creation and annihilation operators gives the following expression:

$$\langle \mathbf{k} | H' | \mathbf{k'} \rangle^2 = \frac{\hbar^2}{M^2 \omega^2} C^2(\mathbf{k}, \mathbf{k'}) [N(N' + 1) - N'(N + 1)],$$
$$(B3)$$

where N refers to the number of phonons in a given state.

It has been shown that the term in square brackets reduces to 1 in the integral over the constant energy surface corresponding to final $\mathbf{k}'$ states [5].

Here the coefficient (C) is calculated for the mass-difference case, in which the perturbation stems from an atom with mass $M' = M_0 + \Delta M$ sitting at site $\mathbf{R}$. The perturbations due to force-constant fluctuation and strain are similar in form. The energy perturbation (E') to the lattice due to mass difference comes in through the kinetic energy term

$$E'(\mathbf{R}) = \frac{1}{2} \Delta M(\mathbf{R}) \dot{u}^2(\mathbf{R}), \qquad (B4)$$

where $\dot{u}(\mathbf{R})$ signifies the time derivative of the unit-cell displacement:

The real-space perturbation is written in terms of a reciprocal-space vector ($\mathbf{Q}$) by taking the Fourier transform:

$$\Delta \tilde{M}(\mathbf{Q}) = \frac{1}{S} \sum_{\mathbf{R}} \Delta M(\mathbf{R}) e^{i\mathbf{Q}\mathbf{R}}, \qquad (B5)$$

where S refers to the number of sites in the lattice [23,25].

The expression for C^2 picks up a factor of $\Delta \tilde{M}(\mathbf{Q}) \Delta \tilde{M}(\mathbf{Q}')$, which is given by

$$\Delta \tilde{M}(\mathbf{Q}) \Delta \tilde{M}(\mathbf{Q}') = \frac{1}{S^2} \sum_{\mathbf{R},\mathbf{R}'} \Delta M(\mathbf{R}) \Delta M(\mathbf{R}') e^{i(\mathbf{Q}'\mathbf{R}'-\mathbf{Q}\mathbf{R})}. \qquad (B6)$$

If the approximation is made that the point defects are randomly distributed over the lattice, the sum over lattice sites can instead be written as an average squared mass difference (ΔM^2) times the number of defect sites in the lattice (S_i) [23,25]:

$$\Delta \tilde{M}(\mathbf{Q}) \Delta \tilde{M}(\mathbf{Q}') = \frac{1}{S} \frac{S_i}{S} \Delta M^2 = \frac{1}{S} f_i \Delta M^2. \qquad (B7)$$

The velocity $\dot{u}$ is again written in terms of creation and annihilation operators, which contribute a frequency and polarization-vector dependence to yield the full expression for C^2 [42]:

$$C^2 = \frac{1}{4S} f_i (\Delta M)^2 \omega^4 |[\mathbf{e}_\mathbf{k}(s) \cdot \mathbf{e}_{\mathbf{k}'}(s)]|^2. \qquad (B8)$$

Equation (B8) can then be substituted into Eq. (B1) for the transition probability to obtain the simplified expression shown below:

$$W_{\mathbf{k},\mathbf{k}'} = \frac{\pi}{2S} f_i \frac{\Delta M^2}{M^2} \omega^2 \delta(\Delta \omega) |[\mathbf{e}_\mathbf{k}(s) \cdot \mathbf{e}_{\mathbf{k}'}(s)]|^2. \qquad (B9)$$

To get the scattering rate, one must then sum $W_{\mathbf{k},\mathbf{k}'}$ over all possible final phonon states $\mathbf{k}'$. Given the conservation-of-momentum constraint ($|\mathbf{k}| = |\mathbf{k}'|$), this constitutes an integral over a constant-energy surface or sphere of radius k in k space. In the conversion from a sum over discrete k states to an integral over k states, a volume factor of $V_{\text{tot}}/(2\pi)^3$ is picked up, where V_{tot} is the volume of the crystal:

$$\tau_{\text{PD}}^{-1} = \frac{V_{\text{tot}}}{(2\pi)^3} \int W_{\mathbf{k},\mathbf{k}'} d^3\mathbf{k}'. \qquad (B10)$$

The spherical surface integral is evaluated noting that (i) $d^3\mathbf{k}' = k'^2 \sin\Theta dk d\Theta d\phi$, (ii) $\omega_k = \omega_{k'} = v_p(\omega)k'$, (iii) $\int \sin\Theta dk d\Theta d\phi = 4\pi$, (iv) $\delta(\Delta\omega) = \delta(\Delta k)/v_g(\omega)$, and (v) $V_0 = V_{\text{tot}}/S$ is the volume per site:

$$\tau_{\text{PD}}^{-1} = \frac{V_0}{4\pi} f_i \left(\frac{\Delta M}{M}\right)^2 |[\mathbf{e}_\mathbf{k}(s) \cdot \mathbf{e}_{\mathbf{k}'}(s)]|^2 \frac{\omega^4}{v_p^2(\omega)v_g(\omega)}. \qquad (B11)$$

Finally, the relaxation time can be written in terms of the three-dimensional phonon density of states [$g(\omega)$] given in Eq. (12):

$$\tau_{\text{PD}}^{-1} = \frac{\pi V_0}{6} f_i \left(\frac{\Delta M}{M}\right)^2 |[\mathbf{e}_\mathbf{k}(s) \cdot \mathbf{e}_{\mathbf{k}'}(s)]|^2 g(\omega)\omega^2. \qquad (B12)$$

As discussed before in relation to the Tamura model (Sec. II A), the scattering parameter $\Gamma = f_i (\Delta M/M)^2 |[\mathbf{e}_\mathbf{k}(s) \cdot \mathbf{e}_{\mathbf{k}'}(s)]|^2$ Substituting Γ into the equation and setting $V_0 = V_{\text{at}}$ in accordance with the virtual crystal approximation, Eq. (12) is reproduced:

$$\tau_{\text{PD}}^{-1} = \frac{V_0 \pi \Gamma \omega^2 g(\omega)}{6}. \qquad (B13)$$

2. Umklapp scattering

The umklapp scattering rate follows a similar derivation; however, the conservation rule is more complicated since the process involves three phonon modes ($\mathbf{k}, \mathbf{k}', \mathbf{k}''$) as well as momentum exchange with the lattice via the addition or subtraction of a reciprocal-lattice vector ($\mathbf{b}$). The derivation here is adopted from the derivation of Klemens for strain scattering off a point defect; however, in this case, the strain is produced by another phonon rather than a point imperfection [42].

$$\mathbf{k} + \mathbf{b} = \mathbf{k}' + \mathbf{k}''. \qquad (B14)$$

The umklapp perturbation-matrix element is similar in form to that of point-defect scattering, but now includes three creation or annihilation operators since the process involves the change in occupation number for three

phonon modes. Additionally, the coefficient (C_U) is dependent on the anharmonicity of the lattice:

$$\langle i| H' |f \rangle^2 = [C_U(\mathbf{k}, \mathbf{k}', \mathbf{k}'')a(k)a^*(k')a^*(k'')]^2$$

$$= \frac{\hbar^3}{M^3\omega\omega'\omega''}C_U^2(\mathbf{k}, \mathbf{k}', \mathbf{k}'')$$

$$\times [(N+1)(N'+1)(N''+1) - NN'N''].$$
(B15)

In the Klemens model, the phonon mode k'' is treated as a Fourier strain component producing a perturbation of the lattice energy. If a uniform dilatational strain (Δ) is assumed, the Fourier component can be written as $i\omega''/v_p(\omega'')\sqrt{S}$ in the limit $k'' \rightarrow 0$. The elastic strain impacts force constants, and therefore induces a frequency shift modeled with use of the Grüneisen model [42]:

$$\omega(\mathbf{k}) = \omega_0(\mathbf{k})[1 - \gamma(\mathbf{k})\Delta].$$
(B16)

The coefficient C_U then represents the lattice-energy change associated with a uniform dilatational strain, defined with use of the Grüneisen model, and the form of the uniform dilatation as k'' approaches 0:

$$C_U(\mathbf{k}, \mathbf{k}', \mathbf{k}'') = \frac{-2i}{\sqrt{S}v_p(k'')}\gamma M\omega\omega'\omega''.$$
(B17)

The final component of the squared matrix element [shown in Eq. (B15)] is the term in square brackets, representing the difference in occupation of phonon modes from the initial state to the final state. In the high-temperature limit, this term can be written in terms of the Bose-Einstein distribution such that it reduces to $k_BT\omega/\hbar\omega'\omega''$. The full form of the squared matrix element simplifies to the following form:

$$\langle i| H' |f \rangle^2 = \frac{\hbar^2}{M} \frac{4\gamma^2\omega^2}{Sv_p^2(k'')}k_BT.$$
(B18)

Just as before, the scattering probability is defined with use of Fermi's golden rule [Eq. (B1)], where the initial and final states are now represented as $|i\rangle$ and $|f\rangle$ for simplicity. As before, the scattering rate is calculated by summing over $W_{i,f}$ for all possible final states. This is achieved by performing a sum over all $\mathbf{k}'$ and $\mathbf{b}$, which then fixes the value of $\mathbf{k}''$ as a result of the conservation condition [Eq. (B14)]:

$$\tau_u = \sum_{\mathbf{k}',\mathbf{b}} W_{i,f}.$$
(B19)

It is assumed that $\mathbf{k}'$ is restricted to spheres of radius $\frac{1}{2}(k + b)$, which is suggested to be true as long as the dispersion relation is not modified by the zone structure [55].

Therefore, the sum can be once again replaced by a surface integral over this sphere, and picks up a volume factor of $V_{\text{tot}}/(2\pi^3)$, where V_{tot} is the volume of the crystal:

$$\tau_u^{-1} = \sum_{\mathbf{b}} \frac{V_{\text{tot}}}{(2\pi)^3} \int W_{i,f}\, d^3\mathbf{k}'.$$
(B20)

Following the same integral simplifications discussed in the derivation of τ_{PD}, the scattering rate due to umklapp processes is as follows:

$$\tau_u^{-1} = \frac{V_0\pi\gamma^2\omega^2}{Mv_p^2(\omega'')v_g(\omega')} \sum_{\mathbf{b}}(k + b)^2.$$
(B21)

Finally, the approximation is made that k is small in magnitude in comparison with the reciprocal-lattice vector $b = 2\pi/a$ such that $(k + b)^2 = 4\pi^2/a^2$. For a cubic-close-packed material with a rhombohedral primitive unit cell, the volume per site V_0 is $a^3(\sqrt{2})^{-1}$, and the scattering rate reduces to the following form:

$$\tau_u^{-1} = \frac{4\pi a\gamma^2 Tk_B}{\sqrt{2}M} \frac{\omega^2}{v_p^2(\omega)v_g(\omega'')}.$$
(B22)

APPENDIX C: DERIVATION OF THE ARCTAN EQUATION

The lattice thermal conductivity with umklapp and point-defect scattering simplifies to a popular function with the form $\tan^{-1}$. The derivation of this form is shown here to highlight the cancellation of phonon velocities in the relaxation times.

Equation (7) gives an expression for the lattice thermal conductivity in terms of the frequency-dependent heat capacity, phonon group velocity, and phonon lifetime, which is reproduced as follows:

$$\kappa = \frac{1}{3} \int_0^{\omega_m} C_s(\omega)v_g(\omega)^2\tau(\omega)d\omega.$$
(C1)

In the high-temperature limit it can be simplified to the following form:

$$\kappa = \frac{k_B}{2\pi^2} \int_0^{\omega_{\text{max}}} \frac{\omega^2}{v_p^2(\omega)v_g(\omega)} v_g^2(\omega) \frac{\tau_u}{1 + \tau_u/\tau_{\text{PD}}}d\omega.$$
(C2)

Next, the phonon velocities are pulled out of the coefficients of the relaxation times [$A = a(v_p^2 v_g)^{-1}$,

$B = b(v_p^2 v_g)^{-1}$]:

$$\kappa = \frac{k_B}{2\pi^2} \int_0^{\omega_{max}} v_g^2(\omega) \frac{1}{v_g(\omega) v_p^2(\omega)} \omega^2$$

$$\times \frac{[1/b(v_p^2 v_g)^{-1}]\omega^2}{1 + a(v_p^2 v_g)^{-1}\omega^2/b(v_p^2 v_g)^{-1}} d\omega. \quad (C3)$$

The phonon velocities in the specific heat, umklapp relaxation time, and the point-defect relaxation time will cancel to yield the final simplified form:

$$\kappa = \frac{k_B}{2\pi^2 b} \int_0^{\omega_{max}} v_g^2(\omega) \frac{1}{1 + a\omega^2/b} d\omega. \quad (C4)$$

If the approximation can be made that the factor v_g^2 is largely frequency independent, then the integral above has a solution in the form of $\tan^{-1}$:

$$\kappa = \frac{k_B v_g^2}{2\pi^2 b(b/a)^{1/2}} \tan^{-1}\left[\frac{\omega_{max}}{(b/a)^{1/2}}\right]. \quad (C5)$$

The pure-lattice thermal conductivity κ_0 can be calculated from Eq. (C4) when the point-defect scattering coefficient a is set to 0. The resulting value of the pure-lattice thermal conductivity κ_0 is $(k_B v_g^2 \omega_{max})/(2\pi^2 b)$. Therefore, the κ_D/κ_0 ratio simplifies to the following form:

$$\frac{\kappa}{\kappa_0} = \frac{\tan^{-1} u}{u}, \quad u = \frac{\omega_{max}}{(b/a)^{1/2}}. \quad (C6)$$

APPENDIX D: PRIMITIVE-UNIT-CELL MASS-DIFFERENCE MODEL

The primitive-unit-cell mass-difference model describes a system in which all individual atom sites in a primitive unit cell are coarse grained into a single, vibrating mass. Therefore, all quantities are defined on a per-unit-cell basis. The parameter can be defined through a statistical mechanics model, where the lattice can be described as a sum of microstates, which represent the unit cells in the lattice. Therefore, the full mass-difference parameter is determined by taking the mass difference of each microstate weighted by the probability of finding that microstate in the lattice (P_{mic}):

$$\Gamma = \sum_{mic} P_{mic} \Gamma_{mic}. \quad (D1)$$

In the case that impurities are randomly distributed on a given sublattice, the probabilities can be calculated with use of the binomial-distribution theorem. As an example, say there is a host compound $A_x B_y C_z$ with impurities A', B', and C', which substitute in the A, B, and C

sublattices, respectively. If f_i is the atomic site fraction of the ith impurity as before, then the overall composition of the alloy is given by $[A(1-f_a)A'(f_a)]_x[B(1-f_b)B'(f_b)]_y[C(1-f_c)C'(f_c)]_z$.

The various microstates that may compose this lattice can be defined by all possible fillings of the A, B, and C sublattices with host atoms versus impurity atoms. Thus, each sublattice is treated as a binomial distribution in which a number of sites (set by the stoichiometry) can each have one of two outcomes: the site can be occupied by an impurity atom with a probability of f_i or it can be occupied by a host atom with a probability of $(1-f_i)$. By the binomial-distribution formula, the probability that r of the total x sites on the A sublattice will be replaced by impurity atoms is given by $\binom{x}{r} f_A^r (1-f_A)^{x-r}$.

Now, it is possible to consider the probability of an example microstate (P_{mic}) such as a unit cell with two impurity atoms in the A sublattice, one impurity atom in the B sublattice, and no impurity atoms in the C sublattice. This full probability would have the following form:

$$P_{mic} = P_A(2)P_B(1)P_C(0), \quad (D2)$$

$$P_{mic} = \left[\binom{x}{2} f_A^2 (1-f_A)^{x-2}\right]\left[\binom{y}{1} f_B^1 (1-f_B)^{y-1}\right]$$

$$\times \left[\binom{z}{0} f_C^0 (1-f_C)^z\right], \quad (D3)$$

where the shorthand $P_A(2)$ refers to the probability of having two impurity atoms in the A sublattice. Γ associated with that microstate would be based on the difference between the mass of that specific microstate (M_m) and the average mass of a unit cell in the lattice. So, for the example microstate above, Γ would have the following form:

$$\Gamma_{mic} = \left(1 - \frac{M_{mic}}{\overline{M}}\right)^2, \quad (D4)$$

$$M_{mic} = M_A(x-2) + M_{A'}(2)$$
$$+ M_B(y-1) + M_{B'} + M_C(z). \quad (D5)$$

APPENDIX E: ELABORATED EXAMPLE OF VACANCY SCATTERING

This section provides a full example of the vacancy-scattering model applied to literature values. The thermal-conductivity measurements from Wang *et al.* [44] are used for $La_{1-x}CoO_{3-y}$ with La and O vacancies. The mass-difference scattering strength is given by the following expression:

$$\Gamma_M = \frac{(1/5)\{x(0-\overline{M_1})^2 + (1-x)(M_{La}-\overline{M_1})^2 + 3[y(0-\overline{M_3})^2 + (1-y)(M_O-\overline{M_3})^2]\}}{\langle \overline{M} \rangle^2}, \tag{E1}$$

where $\overline{M_1}$ is the average mass of the La site and $\overline{M_3}$ is the average mass of the O site. Here the average atomic mass in the compound $\langle \overline{M} \rangle = (\overline{M_1} + M_{Co} + 3\overline{M_3})/5$.

In the original text by Wang *et al.* [44], the full thermal-conductivity reduction is explained using mass-difference scattering alone, without the perturbation due to broken bonds. However, in this case, the volume in Eq. (12) was incorrectly defined as the volume of the primitive unit

cell when defining the point-defect relaxation, whereas it should have been defined as the volume per atom. This error compensates for the missing broken-bond term, such that the curve reported in the paper still adequately represents the data, and the main conclusions about the point-defect scattering strength hold. However, by virial-theorem treatment, the above equation can be adjusted by tripling the mass difference on both vacancy sites as shown below:

$$\Gamma_M = \frac{(1/5)\{x(-M_{La}-2\langle \overline{M} \rangle)^2 + (1-x)(M_{La}-\overline{M_1})^2 + 3[y(-M_O-2\langle \overline{M} \rangle)^2 + (1-y)(M_O-\overline{M_3})^2]\}}{\langle \overline{M} \rangle^2}. \tag{E2}$$

Figure 6 includes (i) the model in the original paper by Wang *et al.* [44] using the unit-cell volume (V_{UC}), (ii) the revised mass-difference-only model, where the volume per atom (V_0) is used, and (iii) the model with the virial-theorem treatment for broken bonds, where V_0 is used. As in the original paper by Wang *et al.* [44], it is assumed that $x = y$ in the defect chemical formula.
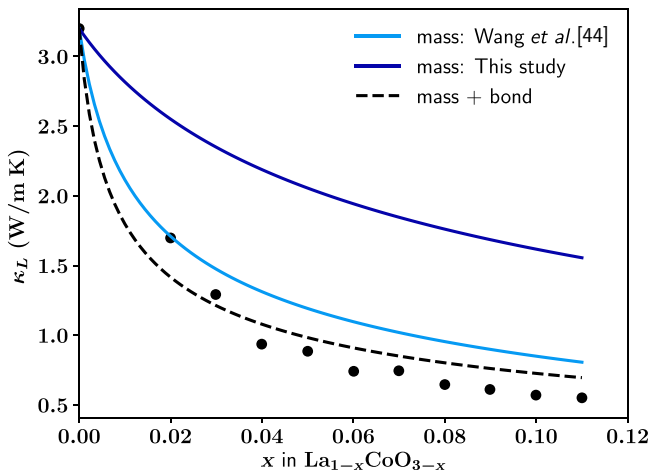

FIG. 6. The mass-difference model with the unit-cell volume error is compared with the mass-difference-only model described in this study as well as the vacancy model with virial-theorem treatment for broken bonds, which best captures the κ_L reduction [44].

[1] H. Wang, A. D. Lalonde, Y. Pei, and G. J. Snyder, The criteria for beneficial disorder in thermoelectric solid solutions, Adv. Funct. Mater. **23**, 1 (2012).

[2] E. S. Toberer, A. Zevalkink, and G. J. Snyder, Phonon engineering through crystal chemistry, J. Mater. Chem. **21**, 15843 (2011).

[3] R. Peierls, *Quanum Theory of Solids* (Oxford University Press, London, 1955), p. 125.

[4] J. Callaway, Model for lattice thermal conductivity at low temperatures, Phys. Rev. **113**, 1046 (1959).

[5] P. G. Klemens, The scattering of low-frequency lattice waves by static imperfections, Proc. Phys. Soc. London, Sect. A **68**, 1113 (1955).

[6] P. Klemens, Thermal resistance due to point defects at high temperatures, Phys. Rev. **119**, 507 (1960).

[7] H. J. Goldsmid, Recent studies of bismuth telluride and its alloys, J. Appl. Phys. **32**, 2198 (1961).

[8] G. P. Meisner, D. T. Morelli, S. Hu, J. Yang, and C. Uher, Structure and Lattice Thermal Conductivity of Fractionally Filled Skutterudites: Solid Solutions of Fully Filled and Unfilled End Members, Phys. Rev. Lett. **80**, 3551 (1998).

[9] J. Yang, G. P. Meisner, and L. Chen, Strain field fluctuation effects on lattice thermal conductivity of ZrNiSn-based thermoelectric compounds, Appl. Phys. Lett. **85**, 1140 (2004).

[10] M. Wood, U. Aydemir, S. Ohno, and G. J. Snyder, Observation of valence band crossing: The thermoelectric properties of $CaZn_2Sb_2$-$CaMg_2Sb_2$ solid solution, J. Mater. Chem. A **6**, 9437 (2018).

[11] E. S. Toberer, A. F. May, B. C. Melot, E. Flage-Larsen, and G. J. Snyder, Electronic structure and transport in thermoelectric compounds AZn_2Sb_2 (A = Sr, Ca, Yb, Eu), Dalton Trans. **39**, 1046 (2010).

[12] A. Katre, J. Carrete, and N. Mingo, Unraveling the dominant phonon scattering mechanism in the thermoelectric compound in ZrNiSn, J. Mater. Chem. A **4,** 15940 (2016).

[13] A. Katre, J. Carrete, T. Wang, G. K. H. Madsen, and N. Mingo, Phonon transport unveils the prevalent point defects in GaN, Phys. Rev. Mater. **2,** 050602 (2018).

[14] W. Li, L. Lindsay, D. A. Broido, D. A. Stewart, and N. Mingo, Thermal conductivity of bulk and nanowire $Mg_2Si_xSn_{1-x}$ alloys from first principles, Phys. Rev. B: Condens. Matter **86,** 174307 (2012).

[15] A. Katre, J. Carrete, B. Dongre, G. K. H. Madsen, and N. Mingo, Exceptionally Strong Phonon Scattering by B Substitution in Cubic SiC, Phys. Rev. Lett. **119,** 075902 (2017).

[16] C. A. Polanco and L. Lindsay, Thermal conductivity of InN with point defects from first principles, Phys. Rev. B **98,** 014306 (2018).

[17] N. Mingo, K. Esfarjani, D. A. Broido, and D. A. Stewart, Cluster scattering effects on phonon conduction in graphene, Phys. Rev. B: Condens. Matter **81,** 045408 (2010).

[18] M. Schrade and T. G. Finstad, Using the callaway model to deduce relevant phonon scattering processes: The importance of phonon dispersion, Phys. Status Solidi (B) **255,** 1800208 (2018).

[19] T. Shiga, T. Hori, and J. Shiomi, Influence of mass contrast in alloy phonon scattering, Jpn. J. Appl. Phys. **53,** 021802 (2014).

[20] T. Feng, B. Qiu, and X. Ruan, Coupling between phonon-phonon and phonon-impurity scattering: A critical revisit of the spectral Matthiessen's rule, Phys. Rev. B: Condens. Matter **92,** 235206 (2015).

[21] R. Berman, E. Foster, and J. Ziman, The thermal conductivity of dielectric crystals: The effect of isotopes, Proc. R. Soc. Lond. A. Math. Phys. Sci. **237,** 344 (1956).

[22] G. A. Slack, Thermal conducitivity of MgO, Al_2O_3, Mg Al_2O_4, and Fe_3O_4 crystals from 3° to 300 °K, Phys. Rev. **126,** 427 (1962).

[23] S.-I. Tamura, Isotope scattering of large wave-vector phonons in GaS and InSb: Deformation dipole and overlap-shell models, Phys. Rev. B **30,** 849 (1984).

[24] R. Berman, *Thermal Conduction in Solids* (Clarendon Press, Oxford, 1976).

[25] S.-I. Tamura, Isotope scattering of dispersive phonons in Ge, Phys. Rev. B **27,** 858 (1983).

[26] J. M. Larkin and A. J. H. Mcgaughey, Predicting alloy vibrational mode properties using lattice dynamics calculations, molecular dynamics simulations, and the virtual crystal approximation, J. Appl. Phys. **114,** 023507 (2017).

[27] A. Togo and I. Tanaka, First principles phonon calculations in materials science, Scr. Mater. **108,** 1 (2015).

[28] J. Carrete, B. Vermeersch, A. Katre, A. van Roekeghem, T. Wang, G. K. Madsen, and N. Mingo, almaBTE: A solver of the space-time dependent Boltzmann transport equation for phonons in structured materials, Comput. Phys. Commun. **220,** 351 (2019).

[29] W. Li, J. Carrete, N. A. Katcho, and N. Mingo, ShengBTE: A solver of the Boltzmann transport equation for phonons, Comput. Phys. Commun. **185,** 1747 (2014).

[30] F. Deangelis, M. G. Muraleedharan, J. Moon, H. Reza, A. J. Minnich, A. J. H. Mcgaughey, A. Henry, F. Deangelis, M. G. Muraleedharan, J. Moon, F. Deangelis, M. Gopal, J. Moon, and H. Reza, Thermal transport in disordered materials, Nanoscale Microscale Thermophys. Eng. **23,** 81 (2018).

[31] P. B. Allen, J. L. Feldman, J. Fabian, and F. Wooten, Diffusons, locons and propagons: Character of atomic vibrations in amorphous, Philos. Mag. B **79,** 1715 (1999).

[32] H. R. Seyf, L. Yates, T. L. Bougher, S. Graham, B. A. Cola, T. Detchprohm, M.-H. Ji, J. Kim, R. Dupuis, W. Lv, and A. Henry, Rethinking phonons: The issue of disorder, npj Comput. Mater. **3,** 49 (2017).

[33] A. Katre, A. Togo, I. Tanaka, and G. K. Madsen, First principles study of thermal conductivity cross-over in nanostructured zinc-chalcogenides, J. Appl. Phys. **117,** 045102 (2015).

[34] Z. Tian, J. Garg, K. Esfarjani, T. Shiga, J. Shiomi, and G. Chen, Phonon conduction in PbSe, PbTe, and $PbTe_{1-x}Se_x$ from first-principles calculations, Phys. Rev. B: Condens. Matter **85,** 184303 (2012).

[35] V. Zaitsev, E. Tkalenko, and E. Nikitin, Lattice thermal conductivity of Mg_2Si-Mg_2Sn, Mg_2Ge–Mg_2Sn, and Mg_2Si-Mg_2Ge solid solution, Sov. Phys. Solid State **11,** 221 (1969).

[36] H. Kamila, P. Sahu, A. Sankhla, M. Yasseri, H.-N. Pham, T. Dasgupta, E. Mueller, and J. de Boor, Analyzing transport properties of p-type Mg_2Si-Mg_2Sn solid solutions: Optimization of thermoelectric performance and insight into the electronic band structure, J. Mater. Chem. A **7,** 1045 (2019).

[37] P. G. Klemens, Thermal resistance due to isotopic mass variation, Proc. Phys. Soc. **70,** 833 (1957).

[38] H. J. Goldsmid, *Introduction to Thermoelectricity* (Springer US, New York, 2010), 2nd ed., p. 67.

[39] X. Wang, I. Veremchuk, M. Bobnar, U. Burkhardt, J. T. Zhao, and Y. Grin, Sodium substitution in lead telluride, Chem. Mater. **30,** 1362 (2018).

[40] Y. Lee, S. Lee, and G. S. Hwang, Effects of vacancy defects on thermal conductivity in crystalline silicon: A nonequilibrium molecular dynamics study, Phys. Rev. B: Condens. Matter **83,** 125202 (2011).

[41] Q. Zheng, C. A. Polanco, M. H. Du, L. R. Lindsay, M. Chi, J. Yan, and B. C. Sales, Antisite Pairs Suppress the Thermal Conductivity of BAs, Phys. Rev. Lett. **121,** 105901 (2018).

[42] P. G. Klemens, Thermal conductivity and lattice vibrational modes, Solid State Phys.: Adv. Res. Appl. **7,** 1 (1958).

[43] G. A. Slack, Effect of isotopes on low-temperature thermal conducitivity, Phys. Rev. **105,** 829 (1955).

[44] Y. Wang, F. Li, L. Xu, Y. Sui, X. Wang, W. Su, and X. Liu, Large thermal conductivity reduction induced by La/O vacancies in the thermoelectric $LaCoO_3$ system, Inorg. Chem. **50,** 4412 (2011).

[45] Y. Pei and D. T. Morelli, Vacancy phonon scattering in thermoelectric In_2Te_3-InSb solid solutions, Appl. Phys. Lett. **94,** 122112 (2009).

[46] G. Tan, W. G. Zeier, F. Shi, P. Wang, G. Je, V. P. Dravid, and M. G. Kanatzidis, High thermoelectric performance $SnTe$-In_2Te_3 solid solutions enabled by resonant levels and strong vacancy phonon scattering, Chem. Mater. **27,** 7801 (2015).

[47] Z. Qu, T. D. Sparks, W. Pan, and D. R. Clarke, Thermal conductivity of the gadolinium calcium silicate apatites: Effect of different point defect types, Acta. Mater. **59**, 3841 (2011).

[48] P. E. Hopkins, Dispersion considerations affecting phonon-mass impurity scattering rates, AIP Adv. **1**, 041705 (2011).

[49] J. Callaway, Effect of point imperfections on lattice thermal conductivity, Phys. Rev. **120**, 1149 (1960).

[50] P. B. Allen, Improved callaway model for lattice thermal conductivity, Phys. Rev. B **88**, 144302 (2013).

[51] P. Carruthers, Theory of thermal conductivity of solids at low temperatures, Rev. Mod. Phys. **33**, 92 (1961).

[52] B. R. Ortiz, H. Peng, A. Lopez, P. A. Parilla, S. Lany, and E. S. Toberer, Effect of extended strain fields on point defect phonon scattering in thermoelectric materials, Phys. Chem. Chem. Phys. **17**, 19410 (2015).

[53] B. Abeles, Lattice thermal conductivity of disordered semiconductor alloys and high temperatures, Phys. Rev. **131**, 1906 (1963).

[54] M. Zhao, W. Pan, C. Wan, Z. Qu, Z. Li, and J. Yang, Defect engineering in development of low thermal conductivity materials: A review, J. Eur. Ceram. Soc. **37**, 1 (2017).

[55] M. Roufosse and P. Klemens, Thermal conductivity of complex dielectric solids, Phys. Rev. B **7**, 5379 (1976).

[56] J. E. Parrott, The high temperature thermal conductivity of semiconductor alloys, Proc. Phys. Soc. **81**, 726 (1963).

[57] A. Togo, L. Chaput, and I. Tanaka, Distributions of phonon lifetimes in Brillouin zones, Phys. Rev. B **91**, 094306 (2015).

[58] M. T. Agne, R. Hanus, and G. J. Snyder, Minimum thermal conductivity in the context of diffuson-mediated thermal transport, Energy Environm. Sci. **11**, 609 (2018).

[59] B. Klobes, J. de Boor, A. Alatas, M. Y. Hu, R. E. Simon, and R. P. Hermann, Lattice dynamics and elasticity in thermoelectric $Mg_2Si_{1-x}Sn_x$, Phys. Rev. Mater. **3**, 025404 (2019).

[60] Y. Wang, F. Yang, and P. Xiao, Rattlers or oxygen vacancies: Determinant of high temperature plateau thermal conductivity in doped pyrochlores, Appl. Phys. Lett. **102**, 1 (2013).

[61] G. Tan, S. Hao, R. C. Hanus, X. Zhang, S. Anand, T. P. Bailey, A. J. Rettie, X. Su, C. Uher, V. P. Dravid, G. J. Snyder, C. Wolverton, and M. G. Kanatzidis, High thermoelectric performance in $SnTe$-$AgSbTe_2$ alloys from lattice softening, giant phonon- vacancy scattering, and valence band convergence, ACS Energy Lett. **3**, 705 (2018).

[62] J. Shen, X. Zhang, S. Lin, J. Li, Z. Chen, W. Li, and Y. Pei, Vacancy scattering for enhancing the thermoelectric performance of $CuGaTe_2$ solid solutions, J. Mater. Chem. A **4**, 15464 (2016).

[63] F. Böcher, S. P. Culver, J. Peilstöcker, K. S. Weldert, and W. G. Zeier, Vacancy and anti-site disorder scattering in $AgBiSe_2$ thermoelectrics, Dalton Trans. **46**, 3906 (2017).

[64] C. A. Ratsifaritana and P. G. Klemens, Scattering of phonons by vacancies, Int. J. Thermophys. **8**, 737 (1987).

[65] P. G. Klemens, Phonon scattering by oxygen vacancies in ceramics, Phys. B **264**, 263 (1999).

[66] Y. Pei, L. Zheng, W. Li, S. Lin, Z. Chen, Y. Wang, X. Xu, H. Yu, Y. Chen, and B. Ge, Interstitial point defect scattering contributing to high thermoelectric performance in $SnTe$, Adv. Electron. Mater. **2**, 1600019 (2016).